Research Article

NMR IN BIOMEDICINE

Received: 27 November 2011, Revised: 1 March 2012, Accepted: 8 March 2012, Published online in Wiley Online Library: 2012

(wileyonlinelibrary.com) DOI: 10.1002/nbm.2803

Investigation of the effective connectivity of resting state networks in Alzheimer's disease: a functional MRI study combining independent components analysis and multivariate Granger causality analysis

Zhenyu Liu[a†], Yumei Zhang[b†], Lijun Bai[a†], Hao Yan[c], Ruwei Dai[a], Chongguang Zhong[a], Hu Wang[a], Wenjuan Wei[a], Ting Xue[d], Yuanyuan Feng[a], Youbo You[a] and Jie Tian[a,d]*

Recent neuroimaging studies have shown that the cognitive and memory decline in patients with Alzheimer's disease (AD) is coupled with abnormal functions of focal brain regions and disrupted functional connectivity between distinct brain regions, as well as losses in small-world attributes. However, the causal interactions among the spatially isolated, but functionally related, resting state networks (RSNs) are still largely unexplored. In this study, we first identified eight RSNs by independent components analysis from resting state functional MRI data of 18 patients with AD and 18 age-matched healthy subjects. We then performed a multivariate Granger causality analysis (mGCA) to evaluate the effective connectivity among the RSNs. We found that patients with AD exhibited decreased causal interactions among the RSNs in both intensity and quantity relative to normal controls. Results from mGCA indicated that the causal interactions involving the default mode network and auditory network were weaker in patients with AD, whereas stronger causal connectivity emerged in relation to the memory network and executive control network. Our findings suggest that the default mode network plays a less important role in patients with AD. Increased causal connectivity of the memory network and self-referential network may elucidate the dysfunctional and compensatory processes in the brain networks of patients with AD. These preliminary findings may provide a new pathway towards the determination of the neurophysiological mechanisms of AD. Copyright © 2012 John Wiley & Sons, Ltd.

Keywords: Alzheimer's disease; resting state functional MRI; effective connectivity; independent components analysis; multivariate Granger causality analysis

INTRODUCTION

Alzheimer's disease (AD), accounting for 50–60% of all dementia (1), is a progressive, neurodegenerative disorder characterized by significant impairments in multiple cognitive domains, including memory, attention, reasoning, language and executive functions. The pattern of brain pathology in AD evolves as the disease progresses, starting mainly in the hippocampus and entorhinal cortex and subsequently spreading throughout most of the temporal lobe and the posterior cingulate, finally involving extensive brain regions (2–4). Neuroimaging, in particular functional MRI (fMRI), studies of the neuromechanisms of AD have shifted from those

* *Correspondence to: J. Tian, Institute of Automation, Chinese Academy of Sciences, PO Box 2728, Beijing 100190, China. E-mail: tian@ieee.org*

a *Z. Liu, L. Bai, R. Dai, C. Zhong, H. Wang, W. Wei, Y. Feng, Y. You, J. Tian Intelligent Medical Research Center, State Key Laboratory of Management and Control for Complex System, Institute of Automation, Chinese Academy of Sciences, Beijing 100190, China*

b *Y. Zhang Neurology Department, Beijing Tiantan Hospital, affiliated with Capital Medical University, Beijing 100050, China*

c *H. Yan School of Psychology, Shaanxi Normal University, Xi'an 710062, China*

d *T. Xue, J. Tian Life Sciences Research Center, School of Life Sciences and Technology, Xidian University, Xi'an, Shaanxi, 710071, China*

† *These authors contributed equally to this work.*

Abbreviations used: *AD, Alzheimer's disease; AN, auditory network; DAN, dorsal attention network; dDTF, direct directed transfer function; DMN, default mode network; DTF, directed transfer function; ECN, executive control network; fMRI, functional MRI; GCA, Granger causality analysis; IC, independent component; ICA, independent component analysis; MeN, memory network; mGCA, multivariate Granger causality analysis; MoN, motor network; PCC, posterior cingulate cortex; RSNs, resting state networks; SD, standard deviation; SN, salience network; VN, visual network.*

highlighting focal regions of abnormal brain functions [for a review, see ref. (5)] to those focusing on the dysfunctional brain connectivity between spatially distinct brain regions [for a review, see ref. (6)].

Resting state fMRI reflects the neuronal baseline activity of the brain, representing the state of the human brain without goal-directed neuronal action and external input (7), and the resting state functional connectivity in the blood oxygenation level-dependent signal during rest corresponds to consistent functionally relevant resting state networks (RSNs) (8). Resting state fMRI has been used to evaluate brain function by measuring functional connectivity between brain regions (9). Previous studies using seed-based analysis have demonstrated decreased functional connectivity in patients with AD relative to normal controls between the precuneus/posterior cingulate cortex (PCC) and several brain regions, including the (medial) temporal cortex, hippocampus and prefrontal cortex (10–12). Moreover, it is particularly noteworthy that several studies (13,14) using graph theoretical approaches have consistently detected AD-related topological changes relative to normal controls in whole brain networks, especially losses of small-world attributes, characterized by abnormal clustering coefficients and characteristic path lengths, providing additional evidence for the disconnection theory of AD (6). However, few studies have evaluated the relationship between large brain networks in patients with AD. It is assumed that patients with AD may not only have dysfunctional connectivity among distinct brain regions, but that their cognitive deficits may be related to the dysfunction of entire networks of regions failing to properly communicate with one another.

Functional network connectivity has recently been employed to measure the relationships among RSNs separated using independent components analysis (ICA) (15). The data-driven method ICA is effective for the examination of the functional connectivity of brain activity as it can isolate the spatial patterns of functionally related neural networks from the spatial patterns of activity related to artifacts, such as subtle movements, machine noise, and cardiac and respiratory pulsations (8,16,17). Each RSN detected using ICA consists of a spatial map and an associated time course. The temporal dependences among the time courses describe the integrity and intervention of brain areas across large neural networks (15). In the classic functional network connectivity analysis, lag shift correlation has been used. However, this method ignores the fact that the interactions among RSNs are complex, possibly dynamic and directional. A previous study (17) has explored the causal interactions among independent components (ICs) using Granger causality analysis (GCA) in the spectral domain. In this article, we propose an alternative causality analysis based on GCA to evaluate the effective connectivity within the RSNs of patients with AD and normal controls. However, a pair-wise Granger causality framework cannot resolve whether the interaction between two time series is direct or indirect (18). Simulations by Kus *et al.* (19) have shown that pair-wise estimates may yield incorrect results. Meanwhile, we compared pair-wise GCA with multivariate GCA (mGCA) using simulated data, and found that the results from pair-wise GCA may be incorrect. Hence, we introduced mGCA (20) to detect the direct causal relations among multiple RSNs and to discern both the direction and strength of information flow among RSNs.

In this study, we combined ICA and mGCA to investigate the causal interactions among RSNs in patients with AD and in normal controls. We identified consistent RSNs from the two groups using ICA. These RSNs have been proven to be highly reproducible and stable across subjects and sessions (8). Then, mGCA was applied to evaluate the effective connectivity between these RSNs. We hypothesized that patients with AD would exhibit weaker and less causal interactions among RSNs, and we expected that RSNs would play abnormal roles in patients with AD relative to those in normal controls.

MATERIALS AND METHODS

All research procedures were approved by the Tiantan Hospital Subcommittee on Human Studies and were conducted in accordance with the Declaration of Helsinki.

Subjects

From Beijing Tiantan Hospital, we recruited 18 right-handed patients with AD, according to the criteria of the National Institute of Neurological and Communicative Disorders and Stroke–Alzheimer's Disease and Related Disorders Association (21). Eighteen healthy right-handed age-matched subjects recruited from the community served as controls. Prior to the experiment, the purpose of the study was briefly explained to the subjects. The main characteristics of the subjects are reported in Table 1. There was no significant difference in terms of age and sex between the normal controls and patients with AD. Each subject provided written informed consent approved by the Institutional Review Board of the Tiantan Hospital Subcommittee on Human Studies. In the AD group, patients with any neurological or psychiatric illness other than AD, and those taking medications or other substances that would influence the central nervous system, were excluded. In the healthy control group, subjects were excluded if they had any neurological or psychiatric illness, or if they were taking medications or other substances that would influence the central nervous system. For the resting state scans, subjects were instructed simply to rest with their eyes closed, relaxed, but not to fall asleep.

Data acquisition and preprocessing

All experiments were performed on a Siemens Trio 3-T MRI system at Tiantan Hospital of Beijing, China. A custom-built head holder was used to prevent head movements. The resting state scan lasted for 8 min and 20 s, and acquired 250 resting state volumes. Functional MR images were obtained using a gradient echo T_2*-weighted pulse sequence with the following parameters: TR = 2000 ms; TE = 30 ms; matrix, 64 × 64; field of view, 256 × 256 mm^2; flip angle, 85°. Then, 20 slices (6 mm thickness, no gap) oriented parallel to the

Table 1. Subject characteristics

	AD	Controls
n	18	18
Age range (years)	43–76	49–78
Age (mean ± SD) (years)	63.7 ± 8.6	64.9 ± 8.4
Sex (male/female)	9/9	10/8
MMSE score (mean ± SD)	18.1 ± 2.8	29.5 ± 0.5
CDR	1	0

No significant differences ($p < 0.05$) were observed in age or sex between the groups. Significant differences were noted in MMSE scores between the groups ($p < 0.0001$).
AD, patients with Alzheimer's disease; CDR, Clinical Dementia Rating; MMSE, Mini-Mental State Examination.

anterior commissure–posterior commissure line were collected to cover the whole brain. After the functional run, a high-resolution T_1-weighted three-dimensional MRI sequence was used (voxel size, $1 \times 1 \times 1\ mm^3$; no gap; TR = 2100 ms; TE = 3.25 ms; matrix, 256×256; field of view, $230 \times 230\ mm^2$; flip angle, 10°).

All preprocessing steps were carried out using Matlab 7.6.0 (R2008a) (MathWorks Inc., Natick, MA, USA) with Statistical Parametric Mapping 5 software (SPM5, http://www.fil.ion.ac.uk). The first five volumes of each session were discarded to allow for equilibrations of the magnetic field. All the remaining volumes were firstly realigned to correct for head motions using least-squares minimization. None of the subjects had head movements exceeding 2 mm on any axis or head rotations greater than 1°. The image data were further processed with spatial normalization based on the Montreal Neurological Institute space (22), and resampled at 2 mm × 2 mm × 2 mm. Temporal band-pass filtering ($0.01 < f < 0.08$ Hz) was then performed to reduce the effects of the low-frequency drifts and high-frequency noise (23) with REST (24). Finally, the images were smoothed with a 6-mm full width at half-maximum Gaussian kernel.

ICA

We performed a group spatial ICA operation on the preprocessed data of patients with AD and normal controls using the fMRI Toolbox (GIFT, http://icatb.sourceforge.net/). The images were reduced to 40 dimensions using principal component analysis, and the number of ICs was estimated to be 25 using the minimum description length criteria (25). The mean ICs of all the subjects, the corresponding mean time courses and the ICs for each subject were obtained from group ICA separation and back reconstruction (26). The maps of these ICs across all subjects were generated for a random effect analysis using a one-sample *t*-test ($p < 0.05$, correction using the false discovery rate criterion). The intensity values in each spatial map were converted to *Z* scores to indicate the voxels that contributed most strongly to a particular IC. Voxels with absolute *Z* values greater than 1.5 were considered as active voxels of the IC in this study (27). According to previous studies (15,28), a selection of the components to be retained for further analysis among the 25 estimated ICs was performed using anatomic information. The classification of the ICs in terms of RSNs was performed according to the fMRI networks during rest consistently shown in previous ICA studies (29,30). Our selected RSNs corresponded to the cerebral components with the largest spatial correlations with the network templates (31,32), which contained the main components of the RSNs. We then calculated the average *Z* score of active voxels for each selected RSN.

mGCA

mGCA has been proven to be effective for the investigation of causal networks according to previous neuroimaging studies (20,33,34). In the current study, we paid attention to the effective connectivity patterns of patients with AD and normal controls using mGCA. Let $\mathbf{X}(t) = (x_1(t), x_2(t), \ldots, x_N(t))^T$ be a matrix representing data from the summary time series of the ICs. Here, $x_i(t)(i = 1, \ldots, N)$ is a time series corresponding to the *i*th IC and *T* denotes the matrix transposition. In the following, bold letters denote time domain matrices and capital letters in normal font denote their frequency domain counterparts. The multivariate autoregressive model of order *p* is given by:

$$\mathbf{X}(t) - \sum_{n=1}^{p} \mathbf{A}(n)\mathbf{X}(t-n) = \mathbf{E}(t) \quad [1]$$

where $\mathbf{A}(n)$ denotes the matrix of model parameters consisting of elements $a_{ij}(n)$ and $\mathbf{E}(t)$ is the vector corresponding to the residual error. The order of the autoregressive model was set to unity using the Schwarz criterion (20,27,35). Then, Equation [1] is transformed to the frequency domain as follows:

$$X(f) = A^{-1}(f)E(f) = H(f)E(f) \quad [2]$$

$$H(f) = A^{-1}(f) \quad [3]$$

where $a_{ij}(f) = \delta_{ij} - \sum_{n=1}^{p} a_{ij}(n)e^{-i2\pi fn}$ and the element a_{ij} corresponds to the matrix *A*. Here, δ_{ij} is the delta function, expressed as $\delta_{ij} = \begin{cases} 1, & i = j, \\ 0, & i \neq j. \end{cases}$. In addition, $i = 1, \ldots, N$ and $j = 1, \ldots, N$. $H(f)$ is the frequency domain transfer matrix and $h_{ij}(f)$ represents its element in the *i*th row and *j*th column. $h_{ij}(f)$ is defined as the non-normalized directed transfer function (DTF) corresponding to the influence of IC *j* on IC *i* (19). The direct DTF (dDTF) was obtained by multiplying $h_{ij}(f)$ with the partial coherence between ICs *i* and *j*. This operation emphasized the direct causality rather than mediated influences.

To calculate the partial coherence, the cross-spectra was computed as:

$$S(f) = H(f)VH^H(f) \quad [4]$$

Here, *V* is the variance of the matrix $E(f)$ and superscript *H* denotes transposition of the conjugate. Then, we obtained the partial coherence between ICs *i* and *j* using:

$$\theta_{ij}(f) = \frac{M_{ij}^2(f)}{M_{ii}(f)M_{jj}(f)} \quad [5]$$

where $M_{ij}(f)$ is the cofactor of the matrix *S*. The partial coherence was confined to the range [0, 1]. A zero value indicates no direct relation between a pair of ICs in a statistically significant manner. A value of unity indicates that there is complete direct association. dDTF was defined as the sum of all frequency components of the product of the non-normalized DTF and partial coherence as given by:

$$dDTF_{ij} = \sum_f h_{ij}(f)\theta_{ij}(f) \quad [6]$$

Eventually, we obtained the dDTF value, which only reflects the magnitude of the causal influences between ICs. To assess the significance of path weights, a null distribution was obtained by generating 2500 sets of surrogate data and calculating the dDTF from these datasets (36). The dDTF value was compared with the null distribution for a one-tailed test of significance with $p = 0.05$. The effective connectivity network of the eight ICs was constructed by scaling the significant dDTF values.

Node interaction analysis

In order to better extract information on the temporal relations among the RSNs obtained from mGCA, a node interaction analysis was performed. In the current study, we analyzed the measures of 'In degree' and 'Out degree' of the two directed

networks. A general definition of 'In degree' and 'Out degree', as provided by previous studies (37,38), is as follows:

- 'In degree': number of Granger causal efferent connections to a node (one of the RSNs) from any other node. This causal flow profile identifies nodes that are the central targets of the network.
- 'Out degree': number of Granger causal afferent connections from a node (one of the RSNs) to any other node. This causal flow profile identifies nodes that are the central sources of the network.

The nodes with high degree were considered to be the hubs of the network (39). We calculated 'In + Out degree' for every RSN. Further, RSNs were identified as the hubs in the network if their sums of 'In degree' and 'Out degree' were at least one standard deviation (SD) greater than the average 'In + Out degree' for all RSNs (i.e. sum > mean + SD). We calculated the sum of 'In and Out degree' for every subject to explore the difference in the quantity of effective connectivity between patients with AD and normal controls. We then calculated the sum of dDTF values for all connections for every subject to explore the difference in the intensity of effective connectivity between patients with AD and normal controls.

RESULTS

Component selection and analysis

We identified eight ICs for mGCA. The spatial maps of the eight RSNs selected for effective connectivity analysis in normal controls and patients with AD are illustrated in Fig. 1. Tables 2 and 3 summarize the components selected in normal controls and patients with AD, respectively, together with the regions of activation and the Brodmann areas in which activations occurred. On the basis of our results, and those of a large number of RSN studies, the eight ICs associated with RSNs can be described as follows:

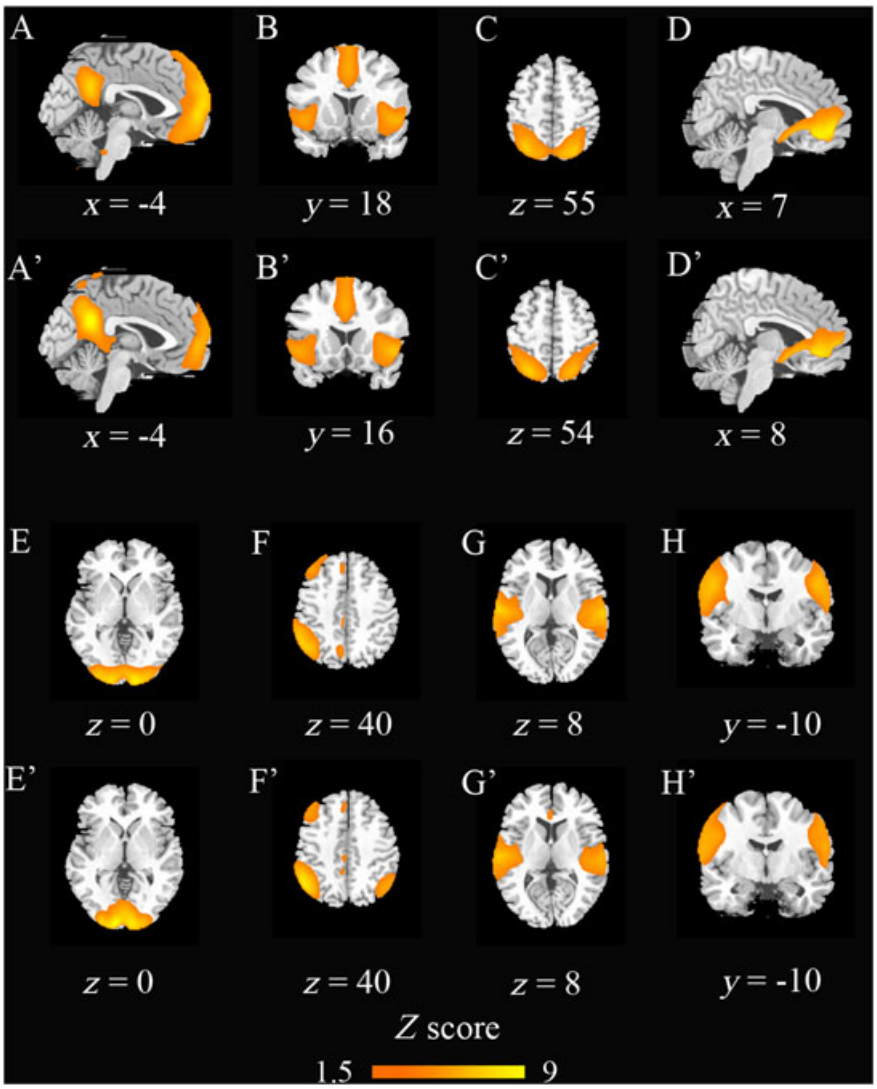

Figure 1. Representation of the eight resting state networks (RSNs) of resting state functional MRI (fMRI) data of patients with Alzheimer's disease (AD) and normal controls. (A–H) DMN, SN, DAN, ECN, VN, MeN, AN and MoN in AD patients. (A'–H') DMN, SN, DAN, ECN, VN, MeN, AN and MoN in normal controls. Images are *Z* statistics overlaid on the average high-resolution scan transformed into standard (Montreal Neurological Institute 152) space. AN, auditory network; DAN, dorsal attention network; DMN, default mode network; ECN, executive control network; MeN, memory network; MoN, motor network; SN, salience network; VN, visual network.

NMR IN BIOMEDICINE

Table 2. Regions activated in normal controls during the resting state (one-sample *t*-test results)

Brain region	Brodmann area	Talairach			Maximal *Z* score	Volume (voxel)
		x	*y*	*z*		
RSN1 (default mode network)						
Angular gyrus	39	−49	−68	33	2.57	85
Cingulate gyrus	31	−8	−45	35	2.14	66
Inferior parietal lobule	39,40	−48	−62	38	4.14	204
Middle temporal gyrus	39	−49	−63	29	3.65	64
Posterior cingulate cortex/precuneus	7,23,31	−2	−52	39	3.85	387
Superior parietal lobule	7	−38	−68	44	2.81	27
Superior temporal gyrus	22,39	−51	−59	29	3.82	114
Supramarginal	40	59	−53	25	2.1	88
RSN2 (salience network)						
Anterior cingulate	24,32	−2	24	23	4.13	244
Cingulate gyrus	32	−2	25	28	4.41	411
Anterior insula	13,47	−42	13	−2	4.17	410
Middle frontal gyrus	9,10	−28	52	21	3.44	216
Superior temporal gyrus	22,38	−48	15	−7	5.32	333
RSN3 (dorsal attention network)						
Inferior parietal lobule	40	38	−52	56	4.4	628
Middle occipital gyrus	19,37	51	−63	−10	2.1	65
Middle temporal gyrus	19,37	55	−55	−9	2.0	50
Superior occipital gyrus	19	−30	−82	26	1.91	42
Superior parietal lobule	7	26	−63	57	6.5	1009
RSN4 (executive control network)						
Anterior cingulate	24,32	4	34	−10	7.79	721
Caudate		−6	13	−6	5.2	210
Inferior frontal gyrus	47	−22	23	−15	5.14	112
Middle frontal gyrus	10,11	−22	25	−15	5.27	70
Medial frontal gyrus	9,10	2	54	−3	6.85	351
Superior frontal gyrus	10	8	56	−1	5.49	132
RSN5 (visual network)						
Cuneus	17,18,19	4	−91	8	7.59	1535
Lingual gyrus	17,18	2	−87	4	7.07	550
Inferior occipital gyrus	17	−10	−92	−7	2.21	8
Middle occipital gyrus	18,19	8	−93	14	6.61	331
RSN6 (memory network)						
Cingulate gyrus	24,31	10	−45	37	1.78	103
Medial frontal gyrus	8,9	4	31	39	1.9	74
Middle frontal gyrus	6,8,9,10	42	48	−11	3.53	674
Middle temporal gyrus	21	65	−31	−5	2.42	126
Superior parietal lobule	7	44	−58	51	8.06	317
RSN7 (auditory network)						
Anterior cingulate	24	2	32	11	2.4	117
Insula	13,40,41	46	−26	14	3.36	573
Middle temporal gyrus	21,22	65	−29	5	2.98	248
Postcentral gyrus	40,43	63	−21	14	4.82	252
Superior temporal gyrus	22,38,41	63	−21	10	5.35	1351
RSN8 (motor network)						
Inferior parietal lobule	40	46	−32	57	4.11	549
Middle frontal gyrus	6,8,9	32	−7	61	2.49	122
Postcentral gyrus	1,2,3,4	40	−28	62	5.16	1475
Precentral gyrus	4,6	38	−28	62	4.76	872
Middle temporal gyrus	37	55	−62	1	1.67	20

- RSN1: the network referred to as the default mode network (DMN) (23,40). This network has been suggested to be involved in internal processing (40,41). It mainly includes the PCC/precuneus region, bilateral inferior parietal gyrus, angular gyrus, middle temporal gyrus and superior temporal gyrus.
- RSN2: the network corresponding to the salience network (SN) for its role in processing diverse homeostatically relevant

Table 3. Regions activated in patients with Alzheimer's disease during the resting state (one-sample *t*-test results)

Brain region	Brodmann area	Talairach			Maximal *Z* score	Volume (voxel)
		x	*y*	*z*		
RSN1 (default mode network)						
Angular gyrus	39	−49	−68	31	2.97	126
Cingulate gyrus	23,24,31	−8	−45	34	3.38	523
Inferior parietal lobule	7,39,40	−42	−66	40	5.39	462
Middle temporal gyrus	39	−48	−63	29	3.37	75
Posterior cingulate cortex/precuneus	7,23,31	−2	−49	25	6.15	1571
Superior parietal lobule	7	−38	−68	44	5.04	189
Superior temporal gyrus	39	−46	−59	29	3.82	56
Supramarginal	40	55	−55	30	2.68	28
RSN2 (salience network)						
Anterior cingulate	24,32	−2	24	23	3.16	141
Cingulate gyrus	32	−2	23	28	3.22	448
Anterior insula	13	40	11	−6	2.04	40
Middle frontal gyrus	10,46	44	49	12	1.65	10
Superior temporal gyrus	22,38,42	−61	−30	20	1.93	44
RSN3 (dorsal attention network)						
Inferior parietal lobule	7,39,40	38	−52	56	4.52	385
Middle occipital gyrus	19,37	−32	−84	21	2.25	88
Middle temporal gyrus	19,37	57	−53	−7	2.45	86
Superior occipital gyrus	19	32	−80	28	2.61	128
Superior parietal lobule	5,7	26	−57	62	6.66	976
RSN4 (executive control network)						
Anterior cingulate	24,32	4	33	−10	7.98	705
Caudate		−4	11	−6	4.83	151
Inferior frontal gyrus	11,47	−20	22	−16	4.4	83
Middle frontal gyrus	10,11	−20	24	−16	4.38	22
Medial frontal gyrus	9,10,11	4	32	−12	8.04	425
Superior frontal gyrus	10	8	54	−1	4.48	41
RSN5 (visual network)						
Cuneus	17,18,19	2	−87	14	6.68	1880
Lingual gyrus	17,18,19	−2	−87	4	5.88	611
Inferior occipital gyrus	17	−10	−91	−7	2.08	44
Middle occipital gyrus	18	8	−93	14	4.42	180
RSN6 (memory network)						
Cingulate gyrus	31	4	−25	42	1.62	13
Medial frontal gyrus	6,8,9	20	64	4	2.07	80
Middle frontal gyrus	8,9,10	36	56	−6	3.61	915
Middle temporal gyrus	21,37,39	61	−49	−8	2.31	90
Superior parietal lobule	7	40	−55	56	7.25	177
RSN7 (auditory network)						
Insula	13,40,41	46	−26	14	2.74	636
Middle temporal gyrus	21,22	−65	−29	5	3.63	308
Postcentral gyrus	40,43	−61	−23	14	4.51	253
Superior temporal gyrus	22,38,41	−63	−21	10	5.53	1833
RSN8 (motor network)						
Inferior parietal lobule	39,40	46	−61	37	4.91	308
Middle frontal gyrus	6,8,9	53	2	39	3.19	122
Postcentral gyrus	1,3,4,43	59	−5	17	4.04	353
Precentral gyrus	6,41	55	−5	17	3.6	1474
Superior temporal gyrus	22	61	−3	9	3.71	127

internal or external stimuli (42). It mainly includes the anterior cingulate, anterior insula and middle frontal gyri.

- RSN3: the network overlapping with the dorsal attention network (DAN), which is thought to mediate goal-directed top–down processing (43,44). It primarily involves the middle and superior occipital gyrus, inferior and superior parietal gyrus, and middle temporal gyrus.
- RSN4: the network putatively associated with the executive control network (ECN). It mainly includes the superior and middle prefrontal cortices, anterior cingulate and ventrolateral

prefrontal cortex, involved in executive control and working memory functions (45,46).
- RSN5: the network dedicated to visual processing (visual network, VN) (47), which includes the lingual gyrus, bilateral occipital cortex and the temporal/occipital regions.
- RSN6: the network related to memory (memory network, MeN) (8), which is responsible for memory functions. It primarily includes the middle frontal gyrus, middle temporal gyrus and superior parietal gyrus.
- RSN7: the network involving the insular cortex, and the middle and superior temporal gyri, responsible for auditory processing (auditory network, AN) (48,49).
- RSN8: the network encompassing the precentral gyrus, postcentral gyrus, middle frontal gyrus and middle temporal gyrus, related to motor function (motor network, MoN) (9).

We compared the average Z scores of active voxels for each selected RSN of patients with AD and normal controls. The average Z scores of active voxels for each selected RSN of the two groups are illustrated in Table 4. The average Z scores of active voxels of DMN were significantly higher in patients with AD compared with those in normal controls ($p < 0.01$). Moreover, the average Z scores of active voxels of SN and MeN in patients with AD were significantly lower than those in normal controls ($p < 0.01$).

Effective connectivity patterns of patients with AD and normal controls

We explored the causal interactions using mGCA among the RSNs detected via ICA in patients with AD and normal controls. The effective connectivity patterns of brain networks are described as directed graphs. The thicknesses of the connecting lines and the directions of the arrows indicate the strengths and directions of the causal influences, respectively. Figure 2 shows the Granger casual connectivity measures within the eight RSNs. Only significant effective connectivities ($p < 0.01$) were divided into four levels (25%, 50%, 75% and 100%) relative to the maximum significant dDTF value and presented in the graphs.

In normal controls (Fig. 2A), DMN was mostly connected with other RSNs. DMN was strongly connected with DAN, SN, MoN and AN. Strong causal interactions were also observed between AN and SN, and AN and DAN. Compared with normal controls, patients with AD (Fig. 2B) showed weaker Granger causal interactions within the RSNs in terms of both intensity and quantity ($p < 0.01$). It was particularly noteworthy that the intensities of the interactions of DMN were weaker, whereas a strong bidirectional regulation was forged between MeN and ECN.

In order to better evaluate the causal interactions among RSNs, we show the 'In degree', 'Out degree' and 'In + Out degree' for every RSN in the two networks in Fig. 3. In normal controls, the mean 'In + Out degree' for every RSN was 4.5 and SD was 2.88. DMN and AN served as hubs according to the standard, and were not only central targets, but also central sources, according to the standards. In patients with AD, the mean 'In + Out degree' for every RSN was 3.25 and SD was 1.83. MeN was identified as the hub in patients with AD. Meanwhile, MeN and AN served as central sources, whereas ECN and MeN served as central targets, in the network in patients with AD.

Table 4. Mean Z scores of active voxels of selected resting state networks (RSNs) in patients with Alzheimer's disease (AD) and normal controls

	AD	Controls
DMN	2.7825 ± 0.1912[1]	2.2908 ± 0.1352[1]
SN	2.2746 ± 0.1035[1]	2.3985 ± 0.1085[1]
DAN	2.6909 ± 0.1708	2.5853 ± 0.1446
ECN	3.0298 ± 0.5502	2.9147 ± 0.3829
VN	2.9772 ± 0.4137	2.9957 ± 0.4416
MeN	2.5565 ± 0.1196[1]	2.7853 ± 0.1705[1]
AN	2.5124 ± 0.1519	2.4511 ± 0.1006
MoN	2.5898 ± 0.3325	2.3036 ± 0.1658

[1]Statistically significant difference at the $p < 0.01$ level.
AN, auditory network; DAN, dorsal attention network; DMN, default mode network; ECN, executive control network; MeN, memory network; MoN, motor network; SN, salience network; VN, visual network.

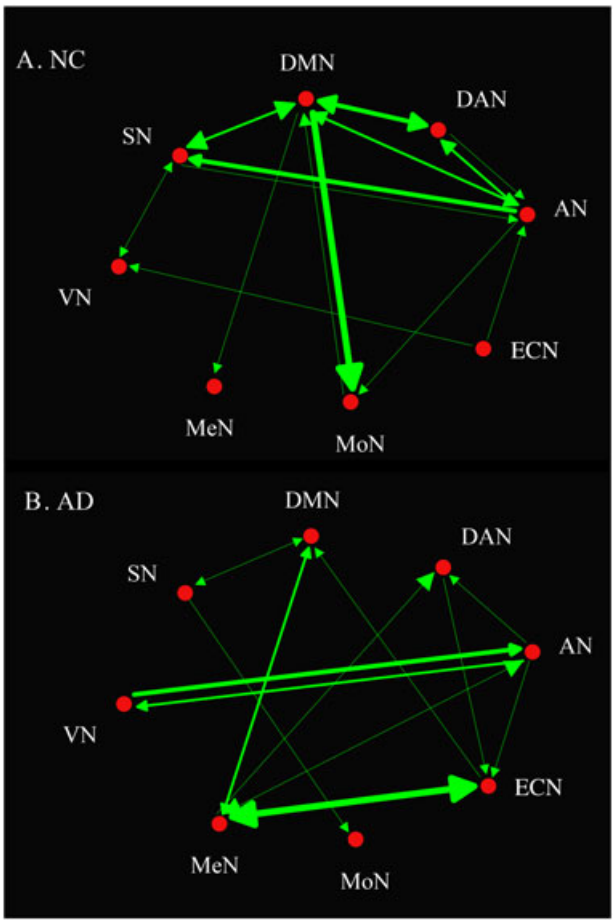

Figure 2. Effective connectivity patterns of patients with Alzheimer's disease (AD) and normal controls (NC) from the multivariate Granger causality analysis (mGCA) result. The red dots refer to the eight resting state networks (RSNs). The relative causal influence strengths were divided into four levels relative to the maximum significant direct directed transfer function (dDTF) value, and are represented by the thicknesses of the green lines. AN, auditory network; DAN, dorsal attention network; DMN, default mode network; ECN, executive control network; MeN, memory network; MoN, motor network; SN, salience network; VN, visual network.

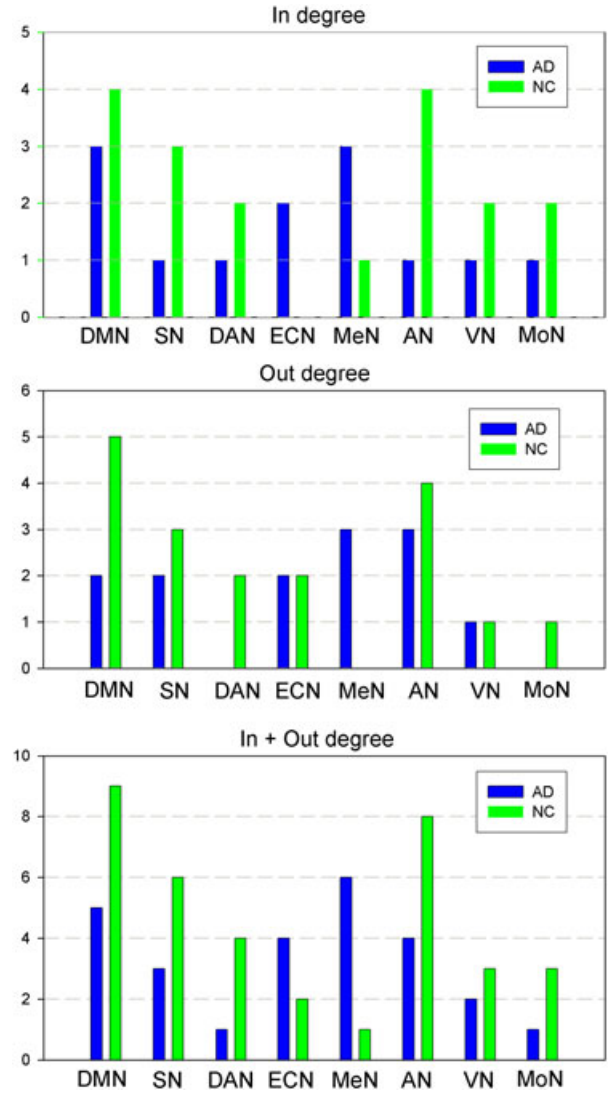

Figure 3. The 'In degree', 'Out degree' and 'In + Out degree' of each resting state network (RSN) in the two multivariate Granger causality analysis (mGCA) networks. A node with high 'In degree' can be considered to be the central target of the network, whereas a node with high 'Out degree' can be considered to be the central source of the network. A node with 'In + Out degree' at least one standard deviation greater than the average 'In + Out degree' for all RSNs was identified as a hub in the network. AD, patients with Alzheimer's disease; AN, auditory network; DAN, dorsal attention network; DMN, default mode network; ECN, executive control network; MeN, memory network; MoN, motor network; NC, normal controls; SN, salience network; VN, visual network.

DISCUSSION

In this study, we combined ICA with mGCA to evaluate the effective connectivity among RSNs of patients with AD and normal controls. The main findings were as follows: (i) compared with normal controls, patients with AD exhibited abnormal effective connectivity patterns; (ii) the causal influence involving DMN and AN was weaker in patients with AD, but stronger causal connectivity emerged in relation to MeN and ECN.

ICA was successfully used to identify resting state components in patients with AD and in normal controls. We were able to examine the causality interactions between these RSNs and to identify their effective connectivity using mGCA. We separated and characterized the activity of eight RSNs, which overlapped with DMN, SN, DAN, ECN, VN, MeN, AN and MoN, as defined previously in neuroimaging studies on active behavior tasks and the resting state (8,9,40,42,43,47,48,50). The DMN reflects an ensemble of cortical regions typically deactivated during demanding cognitive tasks in fMRI studies (40). The DMN has been investigated in various disorders, including AD (10,51–53). SN refers to interoceptive–autonomic processing (54) and homeostatic functions (42), and has been found to show enhanced connectivity in patients with AD (55). DAN appears to be responsible for the preparation and selection for stimuli and responses (43,44). A recent study has suggested that DAN in patients with AD shows decreased intrinsic activity during rest compared with that in normal controls (56). Areas in the ECN have been hypothesized to provide bias signals to other areas of the brain in order to implement cognitive control (45). VN, AN, MeN and MoN relate to visual processing, auditory processing, memory and motor functions, which have been proposed to be brain intrinsic systems. Patients with AD usually show impairments in all of these basic cognitive domains (1).

In addition to identifying the RSNs, the primary purpose of this article was to evaluate their effective connectivity patterns. To date, few studies have paid attention to the causal interactions among RSNs in patients with AD. We found that, in normal controls, DMN shows strong causal interactions with DAN, SN, MoN and AN. However, the effective connectivity between DMN and other RSNs in patients with AD is weaker in both intensity and quantity. Previous studies on AD have found decreased functional connectivity in DMN (10,51). The abnormal connectivity within the DMN and with other regions has been suggested to be directly related to AD (52), and has been proposed as a potential biomarker (51,53). Our findings from mGCA may provide further support for the conclusion that the activity and connectivity in the DMN are weaker in patients with AD (10).

Furthermore, we found that DMN and AN were central targets and central sources in normal controls. A recent fMRI study on DMN has demonstrated that a causal target in the neuronal activity propagation process tends to have a stronger blood oxygenation level-dependent activity, suggesting that causal influences may predict the neuronal activity levels (35). Our results suggest that the DMN is fundamental in the resting state in normal controls, as it can integrate information from other RSNs. However, in patients with AD, DMN was never the hub in the network. We argue that the DMN plays a less important role in patients with AD, as it shows a weaker connectivity. In addition, we found that MeN and AN emerged as central sources and ECN and MeN served as central targets in patients with AD. ECN and DMN have been found to play distinct roles in the human brain functional structure (27). Therefore, we suggest that, when the DMN shows decreased activity and connectivity in patients with AD, ECN may compensate for these impairments. Patients with AD usually show degeneration in basic cognitive domains, such as memory and auditory domains (1). Our results indicate that MeN and AN show greater connectivity in patients with AD, which may reflect the compensatory processes for the two RSNs.

In conclusion, the current investigation focused on the effective connectivity patterns within RSNs in patients with AD and in normal controls. We used ICA to identify RSNs from resting state fMRI data, and mGCA to evaluate the causal interactions among these RSNs. We found that, in patients with AD relative to normal

NMR IN BIOMEDICINE

controls, DMN and AN showed weaker causal interactions with other RSNs, whereas the causal connectivity of MeN and ECN was stronger. This suggests that MeN and ECN may compensate for the impairment of DMN and AN. These preliminary findings may provide a new pathway towards the determination of the neurophysiological mechanisms of AD.

Acknowledgements

This study was supported by the Knowledge Innovation Program of the Chinese Academy of Sciences under Grant No. KGCX2-YW-129, the National Natural Science Foundation of China under Grant Nos. 81071137 and 81071217, the Fundamental Research Funds for the Central University, the Beijing Nova Program and the Project for the National Key Basic Research and Development Program (973) under Grant Nos. 2011CB707700, 2007CB512500, 2007CB512503 and 2009CB521905.

REFERENCES

1. Blennow K, de Leon MJ, Zetterberg H. Alzheimer's disease. Lancet 2006; 368(9533): 387–403.
2. Braak H, Braak E. Evolution of the neuropathology of Alzheimer's disease. Acta Neurol. Scand. Suppl. 1996; 165: 3–12.
3. Jack CR Jr, Shiung MM, Weigand SD, O'Brien PC, Gunter JL, Boeve BF, Knopman DS, Smith GE, Ivnik RJ, Tangalos EG, Petersen RC. Brain atrophy rates predict subsequent clinical conversion in normal elderly and amnestic MCI. Neurology 2005; 65(8): 1227–1231.
4. Thompson PM, Apostolova LG. Computational anatomical methods as applied to ageing and dementia. Br. J. Radiol. 2007; 80(Spec No 2): S78–S91.
5. Dickerson BC, Sperling RA. Neuroimaging biomarkers for clinical trials of disease-modifying therapies in Alzheimer's disease. NeuroRx 2005; 2(2): 348–360.
6. Delbeuck X, Van der Linden M, Collette F. Alzheimer's disease as a disconnection syndrome? Neuropsychol. Rev. 2003; 13(2): 79–92.
7. Scholvinck ML, Maier A, Ye FQ, Duyn JH, Leopold DA. Neural basis of global resting-state fMRI activity. Proc. Natl. Acad. Sci. USA 2010; 107 (22): 10 238–10 243.
8. Damoiseaux JS, Rombouts SA, Barkhof F, Scheltens P, Stam CJ, Smith SM, Beckmann CF. Consistent resting-state networks across healthy subjects. Proc. Natl. Acad. Sci. USA 2006; 103(37): 13 848–13 853.
9. Biswal B, Yetkin FZ, Haughton VM, Hyde JS. Functional connectivity in the motor cortex of resting human brain using echo-planar MRI. Magn. Reson. Med. 1995; 34(4): 537–541.
10. Wang L, Zang Y, He Y, Liang M, Zhang X, Tian L, Wu T, Jiang T, Li K. Changes in hippocampal connectivity in the early stages of Alzheimer's disease: evidence from resting state fMRI. Neuroimage 2006; 31(2): 496–504.
11. Wang K, Liang M, Wang L, Tian L, Zhang X, Li K, Jiang T. Altered functional connectivity in early Alzheimer's disease: a resting-state fMRI study. Hum. Brain Mapp. 2007; 28(10): 967–978.
12. Bai F, Watson DR, Yu H, Shi Y, Yuan Y, Zhang Z. Abnormal resting-state functional connectivity of posterior cingulate cortex in amnestic type mild cognitive impairment. Brain Res. 2009; 1302: 167–174.
13. Supekar K, Menon V, Rubin D, Musen M, Greicius MD. Network analysis of intrinsic functional brain connectivity in Alzheimer's disease. PLoS Comput. Biol. 2008; 4(6): e1000100.
14. Sanz-Arigita EJ, Schoonheim MM, Damoiseaux JS, Rombouts SA, Maris E, Barkhof F, Scheltens P, Stam CJ. Loss of 'small-world' networks in Alzheimer's disease: graph analysis of FMRI resting-state functional connectivity. PLoS One 2010; 5(11): e13788.
15. Jafri MJ, Pearlson GD, Stevens M, Calhoun VD. A method for functional network connectivity among spatially independent resting-state components in schizophrenia. Neuroimage 2008; 39 (4): 1666–1681.
16. McKeown MJ, Jung TP, Makeig S, Brown G, Kindermann SS, Lee TW, Sejnowski TJ. Spatially independent activity patterns in functional MRI data during the stroop color-naming task. Proc. Natl. Acad. Sci. USA 1998; 95(3): 803–810.
17. Demirci O, Stevens MC, Andreasen NC, Michael A, Liu JY, White T, Pearlson GD, Clark VP, Calhoun VD. Investigation of relationships between fMRI brain networks in the spectral domain using ICA and Granger causality reveals distinct differences between schizophrenia patients and healthy controls. Neuroimage 2009; 46(2): 419–431.
18. Granger CWJ. Investigating causal relations by econometric models and cross-spectral methods. Econometrica 1969; 37(3): 424–438.
19. Kus R, Kaminski M, Blinowska KJ. Determination of EEG activity propagation: pair-wise versus multichannel estimate. IEEE Trans. Biomed. Eng. 2004; 51(9): 1501–1510.
20. Deshpande G, LaConte S, James GA, Peltier S, Hu X. Multivariate Granger causality analysis of fMRI data. Hum. Brain Mapp. 2009; 30 (4): 1361–1373.
21. McKhann G, Drachman D, Folstein M, Katzman R, Price D, Stadlan EM. Clinical diagnosis of Alzheimer's disease: report of the NINCDS-ADRDA Work Group under the auspices of Department of Health and Human Services Task Force on Alzheimer's Disease. Neurology 1984; 34(7): 939–944.
22. Ashburner J, Friston KJ. Nonlinear spatial normalization using basis functions. Hum. Brain Mapp. 1999; 7(4): 254–266.
23. Fox MD, Snyder AZ, Vincent JL, Corbetta M, Van Essen DC, Raichle ME. The human brain is intrinsically organized into dynamic, anticorrelated functional networks. Proc. Natl. Acad. Sci. USA 2005; 102(27): 9673–9678.
24. Song XW, Dong ZY, Long XY, Li SF, Zuo XN, Zhu CZ, He Y, Yan CG, Zang YF. REST: a toolkit for resting-state functional magnetic resonance imaging data processing. PLoS One 2011; 6(9): e25031.
25. Li YO, Adah T, Calhoun VD. Sample dependence correction for order selection in fMRI analysis. In *3rd IEEE International Symposium on Biomedical Imaging* 2006; 3: 1072–1075.
26. Calhoun VD, Adali T, Pearlson GD, Pekar JJ. A method for making group inferences from functional MRI data using independent component analysis. Hum. Brain Mapp. 2001; 14(3): 140–151.
27. Liao W, Mantini D, Zhang Z, Pan Z, Ding J, Gong Q, Yang Y, Chen H. Evaluating the effective connectivity of resting state networks using conditional Granger causality. Biol. Cybern. 2010; 102(1): 57–69.
28. Stevens MC, Kiehl KA, Pearlson G, Calhoun VD. Functional neural circuits for mental timekeeping. Hum. Brain Mapp. 2007; 28(5): 394–408.
29. De Luca M, Beckmann CF, De Stefano N, Matthews PM, Smith SM. fMRI resting state networks define distinct modes of long-distance interactions in the human brain. Neuroimage 2006; 29(4): 1359–1367.
30. Mantini D, Perrucci MG, Del Gratta C, Romani GL, Corbetta M. Electrophysiological signatures of resting state networks in the human brain. Proc. Natl. Acad. Sci. USA 2007; 104(32): 13 170–13 175.
31. van de Ven VG, Formisano E, Prvulovic D, Roeder CH, Linden DE. Functional connectivity as revealed by spatial independent component analysis of fMRI measurements during rest. Hum. Brain Mapp. 2004; 22(3): 165–178.
32. van de Ven V, Bledowski C, Prvulovic D, Goebel R, Formisano E, Di Salle F, Linden DE, Esposito F. Visual target modulation of functional connectivity networks revealed by self-organizing group ICA. Hum. Brain Mapp. 2008; 29(12): 1450–1461.
33. Kaminski M, Ding M, Truccolo WA, Bressler SL. Evaluating causal relations in neural systems: Granger causality, directed transfer function and statistical assessment of significance. Biol. Cybern. 2001; 85(2): 145–157.
34. Roebroeck A, Formisano E, Goebel R. Mapping directed influence over the brain using Granger causality and fMRI. Neuroimage 2005; 25(1): 230–242.
35. Jiao Q, Lu G, Zhang Z, Zhong Y, Wang Z, Guo Y, Li K, Ding M, Liu Y. Granger causal influence predicts BOLD activity levels in the default mode network. Hum. Brain Mapp. 2011; 32(1): 154–161.
36. Theiler J, Eubank S, Longtin A, Galdrikian B, Farmer JD. Testing for nonlinearity in time-series -–the method of surrogate data. Physica D 1992; 58(1–4): 77–94.
37. Sridharan D, Levitin DJ, Menon V. A critical role for the right fronto-insular cortex in switching between central-executive and default-mode networks. Proc. Natl. Acad. Sci. USA 2008; 105(34): 12 569–12 574.
38. Stevens MC, Pearlson GD, Calhoun VD. Changes in the interaction of resting-state neural networks from adolescence to adulthood. Hum. Brain Mapp. 2009; 30(8): 2356–2366.
39. Bullmore E, Sporns O. Complex brain networks: graph theoretical analysis of structural and functional systems. Nat. Rev. Neurosci. 2009; 10(3): 186–198.

40. Raichle ME, MacLeod AM, Snyder AZ, Powers WJ, Gusnard DA, Shulman GL. A default mode of brain function. Proc. Natl. Acad. Sci. USA 2001; 98(2): 676–682.
41. Greicius MD, Krasnow B, Reiss AL, Menon V. Functional connectivity in the resting brain: a network analysis of the default mode hypothesis. Proc. Natl. Acad. Sci. USA 2003; 100(1): 253–258.
42. Seeley WW, Menon V, Schatzberg AF, Keller J, Glover GH, Kenna H, Reiss AL, Greicius MD. Dissociable intrinsic connectivity networks for salience processing and executive control. J. Neurosci. 2007; 27 (9): 2349–2356.
43. Corbetta M, Shulman GL. Control of goal-directed and stimulus-driven attention in the brain. Nat. Rev. Neurosci. 2002; 3(3): 201–215.
44. Fox MD, Corbetta M, Snyder AZ, Vincent JL, Raichle ME. Spontaneous neuronal activity distinguishes human dorsal and ventral attention systems. Proc. Natl. Acad. Sci. USA 2006; 103(26): 10 046–10 051.
45. Miller EK, Cohen JD. An integrative theory of prefrontal cortex function. Annu. Rev. Neurosci. 2001; 24: 167–202.
46. Beckmann CF, DeLuca M, Devlin JT, Smith SM. Investigations into resting-state connectivity using independent component analysis. Philos. Trans. R. Soc. B 2005; 360(1457): 1001–1013.
47. Lowe MJ, Mock BJ, Sorenson JA. Functional connectivity in single and multislice echoplanar imaging using resting-state fluctuations. Neuroimage 1998; 7(2): 119–132.
48. Biswal BB, Van Kylen J, Hyde JS. Simultaneous assessment of flow and BOLD signals in resting-state functional connectivity maps. NMR Biomed. 1997; 10(4–5): 165–170.
49. Eckert MA, Kamdar NV, Chang CE, Beckmann CF, Greicius MD, Menon V. A cross-modal system linking primary auditory and visual cortices: evidence from intrinsic fMRI connectivity analysis. Hum. Brain Mapp. 2008; 29(7): 848–857.
50. D'Argembeau A, Collette F, Van der Linden M, Laureys S, Del Fiore G, Degueldre C, Luxen A, Salmon E. Self-referential reflective activity and its relationship with rest: a PET study. Neuroimage 2005; 25 (2): 616–624.
51. Greicius MD, Srivastava G, Reiss AL, Menon V. Default-mode network activity distinguishes Alzheimer's disease from healthy aging: evidence from functional MRI. Proc. Natl. Acad. Sci. USA 2004; 101 (13): 4637–4642.
52. Hedden T, Van Dijk KR, Becker JA, Mehta A, Sperling RA, Johnson KA, Buckner RL. Disruption of functional connectivity in clinically normal older adults harboring amyloid burden. J. Neurosci. 2009; 29(40): 12 686–12 694.
53. Sorg C, Riedl V, Muhlau M, Calhoun VD, Eichele T, Laer L, Drzezga A, Forstl H, Kurz A, Zimmer C, Wohlschlager AM. Selective changes of resting-state networks in individuals at risk for Alzheimer's disease. Proc. Natl. Acad. Sci. USA 2007; 104(47): 18 760–18 765.
54. Fox MD, Snyder AZ, Vincent JL, Corbetta M, Van Essen DC, Raichle ME. The human brain is intrinsically organized into dynamic, anticorrelated functional networks. Proc. Natl. Acad. Sci. USA 2005; 102(27): 9673–9678.
55. Zhou J, Greicius MD, Gennatas ED, Growdon ME, Jang JY, Rabinovici GD, Kramer JH, Weiner M, Miller BL, Seeley WW. Divergent network connectivity changes in behavioural variant frontotemporal dementia and Alzheimer's disease. Brain 2010; 133(Pt 5): 1352–1367.
56. Li R, Wu X, Fleisher AS, Reiman EM, Chen K, Yao L. Attention-related networks in Alzheimer's disease: a resting functional MRI study. Hum. Brain Mapp. 2011; doi:10.1002/hbm.21269.